

## Numerical and experimental study on dynamic response of moored spar-type scale platform for floating offshore wind turbine

E.Y. Choi<sup>1</sup>, J.R. Cho<sup>\*1</sup>, Y.U. Cho<sup>1</sup>, W.B. Jeong<sup>1</sup>, S.B. Lee<sup>1</sup>, S.P. Hong<sup>2</sup>  
and H.H. Chun<sup>2</sup>

<sup>1</sup>*School of Mechanical Engineering, Pusan National University, Busan 609-735, Korea*

<sup>2</sup>*Global Core Research Center for Ships and Offshore Plants, Pusan National University, Busan 609-735, Korea*

*(Received August 4, 2014, Revised December 29, 2014, Accepted March 4, 2015)*

**Abstract.** The dynamic response and the mooring line tension of a 1/75 scale model of spar-type platform for 2.5 MW floating offshore wind turbine subject to one-dimensional regular harmonic wave are investigated numerically and verified by experiment. The upper part of wind turbine which is composed of three rotor blades, hub and nacelle is modeled as a lumped mass the scale model and three mooring lines are pre-tensioned by means of linear springs. The coupled fluid-rigid body interaction is numerically simulated by a coupled FEM-cable dynamics code, while the experiment is performed in a wave tank with the specially-designed vision and data acquisition system. The time responses of surge, heave and pitch motions of the scale platform and the mooring line tensions are obtained numerically and the frequency domain-converted RAOs are compared with the experiment.

**Keywords:** spar-type floating platform; scale model; response amplitude operator (RAO); mooring line tension; fluid-rigid body interaction simulation; wave tank experiment

---

### 1. Introduction

The demand of renewable energies such as solar-, wind- and water-powers and fuel cell is continuously increasing all over the world as natural gas and oil are getting exhausted. Among them, wind power draws a massive attention thanks to its potential to provide the maximum power capacity from plenty of winds around us. Wind turbines were initially designed for installing on land and showed the rapid increase in both the total number of installations and the maximum wind power capacity (Hansen and Hansen 2007). However, such a rapid increase has slowed down due to several obstacles such as the substantial environmental impact on people living in the vicinity of wind turbines and the limitation in making large wind farm. This critical situation naturally turned one's attention to the offshore sites, a less restrictive installation place, which introduced the concept of offshore wind turbine. Offshore wind turbines are basically classified

---

\*Corresponding author, Professor, E-mail: jrcho@pusan.ac.kr

into two categories, fixed- and floating-type according to how the wind turbine tower is supported. Differing from the fixed-type, the floating-type wind turbine is under the concept design stage because several core technologies are not fully settled down (Karimirad *et al.* 2011), particularly the maintenance of the hydrodynamic stability and the dynamic performance against irregular wind, wave and current loads (Faltinsen 1990).

The dynamic performance of floating-type offshore wind turbine at sea is mostly meant by the station keeping and rotational oscillation control (Tong 1998). The former is characterized by surge, sway and heave motions while the latter is by pitch and roll motions. Because of this fundamental requirement at sea, the design of floating-type offshore wind turbine requires extra technologies for designing floating platform, mooring lines or tension legs and anchor system when compared to the fixed-type wind turbines. Floating offshore wind turbines are classified according to how is generated the righting moment or draft control, such as semi-submersible, TLP (tension-leg platform)-, spar-types (Lee 2008, Jonkman 2009, Jeon *et al.* 2013), and barge-type FOWT. However, all the types have some things in common from the fact that the station keeping and the vertical attitude are secured by a combination of the buoyancy force, the tension of mooring lines or tension legs and additional control devices (Lee *et al.* 2006, Colwell and Basu 2009, Mostafa *et al.* 2012).

In case of spar-type floating wind turbine, the buoyancy force produced by a long hollow cylindrical platform supports the whole offshore wind turbine and the mooring tension keeps the station position of spar-type floating substructure. The rotational oscillation is characterized by the pitch and roll motions of floating substructure, which increases in proportional to the metacentric height (i.e., the vertical distance between the metacenter and the center of mass) (Koo *et al.* 2004) and the relative distance between the centers of gravity and buoyancy (Karimirad *et al.* 2011). Karimirad *et al.* considered a single tendon mooring system and noticed that the restoring force from the tendon should be included in the restoring stiffness of the floater in pitch, roll and heave. But, if a catenary mooring system is used, its contribution to the restoring stiffness in these three motion modes is small enough to neglect. Meanwhile, the rotational oscillation is also influenced by both the tension magnitude and the connection position of mooring lines, and it could be improved further when passive tuned liquid damper (TLD) or/and active control using water ballast are employed (Lee 2005, Lee *et al.* 2006, Colwell *et al.* 2009, Seo *et al.* 2012). Here, the pitch and roll stiffness is meant by the pitching and rolling moments required to pitch and roll the substructure by unit angle.

The dynamic response of spar-type offshore wind turbine to wind and wave excitations is usually evaluated in terms of six degrees of freedom of rigid body motions of floating substructure. The station keeping referring to the horizontal degrees of freedom, surge and sway, are largely influenced by the mooring system, while the other degrees of freedom are mainly affected by the floating platform characteristics. This subject has been studied by experimentally using scale models (Nielsen *et al.* 2006, Utsunomiya 2010, Goopee *et al.* 2012, Mostafa *et al.* 2012, Shin and Dam 2012), by analytically/numerically with the simplified wind turbine geometry and the analytically derived wind/wave loads (Tracy 2001, Lee 2005, Karimirad 2010, Jensen *et al.* 2011, Dodaran and Park 2012), or by the combined use of CFD, hydro, FSI (fluid-structure interaction) or/and MBD (multibody dynamics) codes (Zambrano *et al.* 2006, Jonkman 2009, Jonkman and Musial 2010, Wang and Sweetman 2012). Even though the researches on floating offshore wind turbine have been actively conducted, the detailed useful results for the design of spar-type floating platform are still in need of further investigation.

In this context, the current study intends to develop a numerical method for obtaining the

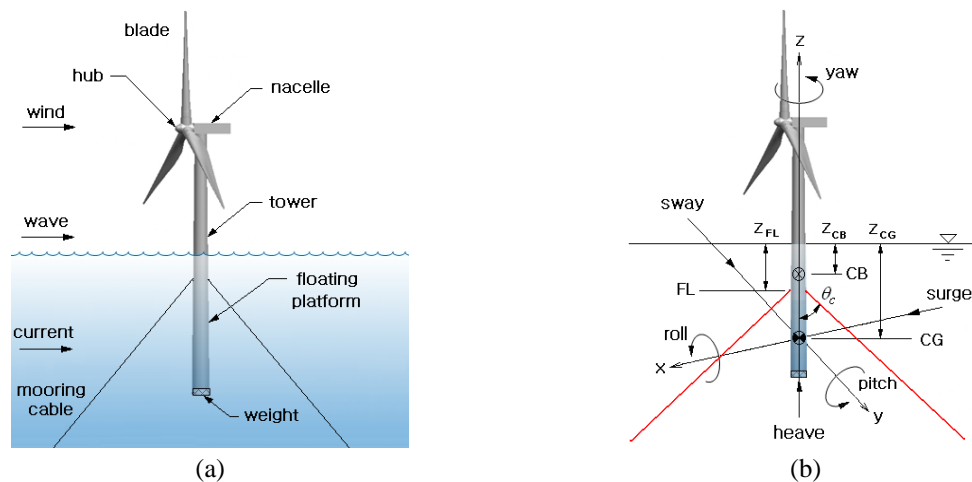


Fig. 1 (a) Spar-type floating offshore wind turbine (b) 6-DOF rigid body motions (CB: center of buoyancy, CG: center of gravity, FL: fairlead)

reliable data of the dynamic response of floating platform and the mooring line tension using a 1/75 scale model for 2.5 MW spar-type floating wind turbine. Since the current study aims at the dynamic response to the wave excitation, the upper part including rotor blades, hub and nacelle is excluded from the scale model, and three mooring lines are pre-tensioned by means of linear springs. The liquid-rigid body interaction simulation of the moored scale model is performed by a coupled FEM-cable dynamics code. As well, the scale model is manufactured and experimented in a wave tank by means of the specially designed sensor and data acquisition system. The time responses of surge, heave and pitch motions are simulated and experimented and their response amplitude operator (RAO) are compared to verify the reliability of the numerical method.

## 2. Spar-type cylindrical floating platform

### 2.1 Spar-type floating offshore wind turbine

A typical spar-type floating offshore wind turbine is represented in Fig. 1(a), where the whole wind turbine is supported by the buoyancy force and the rotational oscillation could be reduced by the bottom weight, tuned liquid damper and hydraulic control. Regarding the dynamic displacement of wind turbine, only surge and sway displacements are counteracted by the mooring lines when a catenary mooring system is adopted while the displacements in all DOFs are counteracted by tension lines if a TLP system is adopted (Lefebvre and Collu 2012). Among several available mooring systems, catenary mooring composed of fabric ropes and steel chains is widely adopted thanks to its topological simplicity and cost effectiveness (Wu 1995). Catenary mooring cables are anchored at seabed and connected to the fairlead of floating platform, and they have small flexural stiffness so that external loads are resisted only by the in-line tension. Here, the external loads include the self weight, the hydrodynamic drag forces in the normal, tangential and bi-normal directions, and the added inertia force stemming from surrounding sea water (Vaz and Patel 2000).

Referring to Fig. 1(b), the rigid body dynamic motion of floating-type wind turbine is expressed in terms of three translational motions, surge, sway and heave and three rigid rotational motions, pitch, roll and yaw. These six rigid body motions are coupled to some extent, and the pitch, roll, surge, sway and heave motions are considered as important factors in the dynamic performance evaluation of floating-type wind turbine. Surge, sway and heave motions influence the station keeping of platform while pitch and roll motions affect the rotational oscillation of platform. The hydrodynamic stability may not only influence the structural safety of the whole wind turbine but also degrade the wind power efficiency, so that it is now intensively investigated by making use of the numerical simulation or/and the scale-model experiment in wave tanks equipped with the wind generation system (Utsunomiya *et al.* 2010, Goopee *et al.* 2012).

The rigid body translational motions of floating platform are characterized by the mooring line tension, which is in turn influenced by the total cable length, the horizontal distance between anchor and platform, the specific weight and stiffness of mooring cables. There is always a fraction of the mooring cables laying on the seabed when the total suspended cable length is not equal to its total length, and such a fraction does not have any influence on the cable tension because its weight is counteracted by the seabed reaction. Thus, the mooring line tension decreases in proportional to the total suspended cable length, and it becomes almost insensitive to the total cable length once the total suspended length reaches a critical portion. Meanwhile, the rigid body rotational motions are influenced by the pitch and roll stiffness of floating platform itself and the fairlead position  $Z_{FL}$ . In general, the pitch and roll stiffness is proportional to the metacentric height, composed of different elements, not only to the distance between the center of buoyancy (CB) and the center of gravity (CG) (Karimirad *et al.* 2011). Furthermore, if the CG is above the CB, then the more distance these points are the less stable is the floating structure. In order to suppress the rotational oscillation, passive tuned liquid damper (TLD) (Lee *et al.* 2006, Colwell and Basu 2009) or active control systems utilizing in-pipe water flow or water jet are in partially used and under development.

## 2.2 Fluid-rigid body interaction

Referring to Fig. 3(a), let us  $\Omega_F \in \mathfrak{R}^3$  be a semi-infinite unbounded flow domain with the boundary  $\partial\Omega_F = S_F \cup S_B \cup \Gamma_I$  and denote  $\mathbf{V}$  be a continuous triple-vector water velocity field, where  $S_F$ ,  $S_B$  and  $\Gamma_I$  indicate the free surface, seabed and flow-structure interface respectively. Water is assumed to be inviscid and incompressible and water flow is irrotational so that there exists a velocity potential function  $\phi(\mathbf{x}; t)$  satisfying

$$\phi(\mathbf{x}; t): \mathbf{V} = \nabla \phi \quad (1)$$

The velocity potential function  $\phi(\mathbf{x}; t)$  is defined by

$$\phi(\mathbf{x}; t) = \sum_{j=1}^6 \phi_j + \phi_w + \phi_d \quad (2)$$

with  $\phi_j$  due to the rigid body motion of structure,  $\phi_w$  due to undisturbed incoming wave and  $\phi_d$  due to diffraction of the undisturbed incoming wave, respectively. Then, the flow field is governed by the continuity equation

$$\nabla^2 \phi = 0, \text{ in } \Omega_F \times (0, \hat{t}] \tag{3}$$

and the boundary conditions given by

$$\frac{\partial \phi}{\partial n} = \dot{\mathbf{u}} \cdot \mathbf{n}, \text{ on } \Gamma_I \tag{4}$$

$$g \frac{\partial \phi}{\partial z} + \frac{\partial^2 \phi}{\partial t^2} = 0, \text{ on } S_F \tag{5}$$

$$\frac{\partial \phi}{\partial z} = 0, \text{ on } S_B \tag{6}$$

with  $\hat{t}$  being the time period of observation,  $\mathbf{u}$  the platform rigid body displacement,  $g$  the gravity acceleration, and  $\mathbf{n}$  the outward unit vector normal to the structure boundary. Eq. (5) is a unified free surface condition derived from the linearized dynamic and kinematic conditions on  $S_F$  by neglecting the surface tension (Cho *et al.* 2005). In addition, the potential function satisfies the radiation condition:  $\phi \rightarrow 0$  as  $r \rightarrow \infty$  at the far field.

The substructure occupying the material domain  $\Omega_S \in \mathbb{R}^3$  with the boundary  $\partial\Omega_S = \Gamma_D \cup \Gamma_N \cup \Gamma_I$  is assumed to be a rigid body. By denoting  $\{\mathbf{d}, \boldsymbol{\theta}\}$  be its rigid body translation and rotation at the center of mass, the dynamic motion of the substructure is governed by the conservation of linear and angular momentums ( $i=x, y, z$ )

$$m \ddot{d}_i + c_i \dot{d}_i + k_i d_i = F_i, \text{ in } \Omega_S \times (0, \hat{t}] \tag{7}$$

$$I_{ij}^{\theta} \ddot{\theta}_j + c_i^{\theta} \dot{\theta}_i + k_i^{\theta} \theta_i = M_i, \text{ in } \Omega_S \times (0, \hat{t}] \tag{8}$$

and the initial conditions given by

$$\{\dot{\mathbf{d}}, \dot{\boldsymbol{\theta}}\}_{t=0} = \{\dot{\mathbf{d}}, \dot{\boldsymbol{\theta}}_0\}, \quad \{\mathbf{d}, \boldsymbol{\theta}\}_{t=0} = \{\mathbf{d}_0, \boldsymbol{\theta}_0\} \tag{9}$$

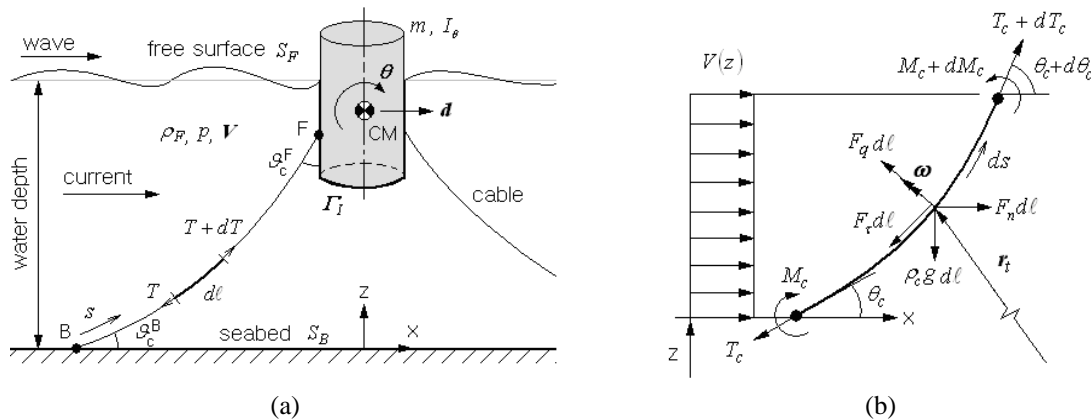


Fig. 2 (a) A rigid floating body moored by catenary cables in irregular wave (b) forces acting on the cable element  $dl$

In which  $m, c_i, k_i, c_i^\theta$  and  $k_i^\theta$  denote the total mass and the damping and stiffness coefficients for the translational and rotational degrees of freedom, respectively. Meanwhile,  $\mathbf{I}^\theta$  indicates the matrix of mass moments of inertia with respect to the center of mass, and  $\mathbf{F}$  and  $\mathbf{M}$  are the external force and moment vectors which are calculated by

$$\mathbf{F} = \int_{\Gamma_i} p \mathbf{n} ds, \quad \mathbf{M} = \int_{\Gamma_i} p \mathbf{r} \times \mathbf{n} ds \quad (10)$$

Here,  $p$  and  $\mathbf{r}$  are the hydrodynamic pressure and the position vector from the center of mass, respectively.

Meanwhile, catenary mooring cable of length  $L$  is a slender flexible structure subject to hydrodynamic pressure, self weight, inertia force and drag force. Referring to Fig. 3(b), the nonlinear differential equations of motion (Goodman and Breslin 1976, Aamo and Fossen 2000) for the differential cable element with the length  $dl$  are governed by the equilibrium equations in translation and rotation

$$(m_c + m_a) \frac{\partial \dot{\mathbf{u}}_c}{\partial t} = \frac{\partial \mathbf{T}_c}{\partial s} + (1 + \gamma) \mathbf{F}_c \quad (11)$$

$$\frac{\partial \mathbf{M}_c}{\partial s} = -\mathbf{r}_t \times (1 + \gamma) \mathbf{T}_c \quad (12)$$

and the compatibility equation

$$\frac{\partial \dot{\mathbf{u}}_c}{\partial s} = \frac{\partial}{\partial t} ((1 + \gamma) \mathbf{r}_t) \quad (13)$$

with the boundary conditions given by

$$\dot{\mathbf{u}}_c = 0, \quad \mathcal{G}_c = \mathcal{G}_c^B \quad \text{at } s = 0 \text{ (at seabed)} \quad (14)$$

$$\dot{\mathbf{u}}_c = \dot{\mathbf{d}}_p, \quad \mathcal{G}_c = \mathcal{G}_c^F \quad \text{at } s = L \text{ (at fairlead)} \quad (15)$$

In which,  $m_c$  indicates the mass per unit arc length,  $m_a$  the added mass of water,  $\dot{\mathbf{u}}_c$  the velocity vector,  $s$  the arc length of unstressed cable, and  $\gamma$  the engineering strain. In addition,  $\mathbf{r}_t$  is the vector tangent to the cable center line,  $\mathbf{M}_c$  the resultant internal moment, and  $\mathbf{F}_c$  the external loading per unit arc length due to the self weight  $\rho_c g$ , and  $\mathbf{F}_n$ ,  $\mathbf{F}_\tau$  and  $\mathbf{F}_q$  the normal, tangential and binormal drag forces (Morison *et al.* 1950). Here, the unit vector  $\mathbf{q}$  in the bi-normal direction is defined by  $\mathbf{q} = \dot{\mathbf{u}}_c \times \boldsymbol{\tau} / |\dot{\mathbf{u}}_c \times \boldsymbol{\tau}|$  with  $\boldsymbol{\tau}$  being the tangential unit vector. Eq. (12) and the associated boundary conditions are excluded when the flexural stiffness of catenary cables is neglected.

The potential flow governed by Eqs. (3)-(6), the dynamic motions of the rigid floating substructure and mooring cables are approximated by the finite element method. For the rigid body dynamic motion analysis, only the surface of rigid floating substructure is discretized with 2-D finite elements and each mooring line is divided into a finite number of line elements. A two-step predictor-corrector method (Cong 1996, Kim and Kim 2001) is used for the time integration of the equations of motion. The Euler-Lagrange-type coupling method is employed to deal with the interaction between the rigid body structure motion and the water flow, and it with the lapse of time is numerically implemented in a staggered iterative manner (Sigrist and Abouri 2006, Cho *et al.* 2008). The hydrodynamic pressure of water flow acts as the external force and moment for

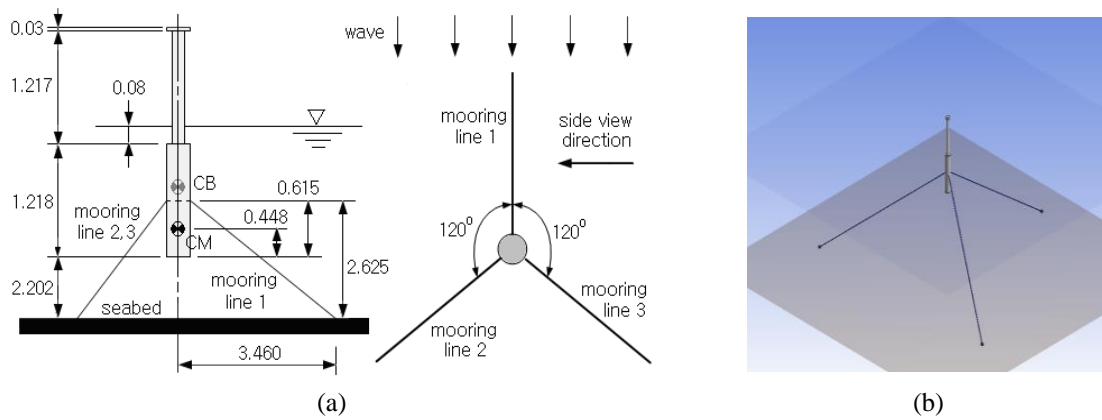


Fig. 3 A simulation problem: (a) simplified moored spar-type platform (scale: 1/75, unit: m) (b) coupled FEM-cable dynamics interaction model

both the floating substructure and mooring cables, and then the rigid body movement of floating substructure relocates the flow-structure interface. This staggered computation iterates up to the preset time period of observation.

### 3. Simulation and experiment using a scale model

#### 3.1 Scale model of spar-type floating platform

A simplified 1/75 scale model of 2.5 MW spar-type floating offshore wind turbine with three equal Nylon mooring lines is taken for investigating the dynamic response of the floating platform and the mooring line tension. The geometry dimensions, masses and moments of inertia of the major components are given in Fig. 3(a) and Table 1. Three rotor blades, hub and nacelle assembly are modeled as a lumped mass for both numerical simulation and wave tank experiment. For the fluid-rigid body interaction simulation, the whole simplified platform is discretized with the total of 10,465 10-node hexahedron elements. The center of buoyancy (CB) and the center of mass (CM) are measured from the bottom of platform and the relative vertical distance between two centers is set by 0.167 m.

In accordance with the dimensions of wave tank, the sectional dimensions of the water pool for the numerical simulation are set by  $8 \times 8$  m and the water depth from is set by 3.5 m, respectively. In the vertical direction, the tower-platform interface is positioned below the free surface by  $0.08$  m and the relative distance between seabed and the platform bottom is set by 2.202 m. The total stretched length of each mooring line and the relative angles between two adjacent mooring lines are set by 4.343 m and  $120^\circ$  respectively. Three mooring lines are equally pre-tensioned by 0.49 kgf and the pre-tension is implemented in the numerical simulation by specifying their initial unstretched length  $L_c^{init}$ . Each mooring line is discretized into 100 uniform elements and fixed at seabed and connected to the platform by the node-to-node connection. The equivalent cross sectional area  $A_c$ , the mass per unit length  $\gamma_c$ , the stiffness  $EA$  and the unstretched initial length  $L_c^{init}$  are set by  $3.14 \times 10^{-6}$  m<sup>2</sup>, 1.1 kg/m,  $2.0 \times 10^2$  N and 4.242 m respectively. The fluid viscous

Table 1 Major specifications of scale platform model

Components	Items	Values
Platform	Diameter (upper & lower)	0.076 m, 0.150 m
	Thickness (upper & lower)	2.9 m, 3.2 m
	Pitch moment of inertia	9.240 kg·m <sup>2</sup>
	Roll moment of inertia	9.237 kg·m <sup>2</sup>
	Yaw moment of inertia	0.065 kg·m <sup>2</sup>
Mooring lines	Spring constant	0.74 kgf/m
	Pretension	0.49 kgf
Tubular Morison element	Diameter	0.151 m
	Thickness	1.0×10 <sup>-3</sup> m
	Mass density	1.0 kg/m <sup>3</sup>

damping effect is reflected by adding a tubular Morison element to the outer surface of lower wet platform, and the associated viscous drag coefficient  $C_d$  and added mass coefficient  $C_{add}$  are set by 0.75 and 1.0. The Morison force is calculated by  $\rho_w D_m C_d (\mathbf{V} - \dot{\mathbf{u}}) |\mathbf{V} - \dot{\mathbf{u}}|$  with  $\rho_w$  and  $D_m$  being the water density and the characteristic diameter of tubular Morison element (Ansys 2012).

Three mooring lines are aligned such that mooring line 1 opposes to the incoming direction of one-dimensional regular harmonic wave as represented in Fig. 3(a), and the amplitude and frequency of regular harmonic wave are set by 1.0 m and 0.5 Hz, respectively. The directions of six components of the rigid body motion of floating offshore wind turbine follow the convention shown in Fig. 1(b). The fluid-rigid body-cable interaction simulation was carried out by the commercial FEM software ANSYS AQWA (Ansys 2012). Note that the anchors are positioned such that there is no fraction of mooring lines laying on the seabed and the mooring lines are modeled as linear cables.

### 3.2 Experimental setup

Figs. 4 and 5 represent the simplified scale platform model, the wave tank and the data acquisition system used for the experiment. The wave tank used for the model test is 100 m in length, 8 m in width, and 3.5 m in depth, and the scale platform model is moored at 30 m downstream of the wave generator and a wave gauge is used to measure the wave elevation. On the right side of the wave tank, three cameras in the vision system and a data acquisition system are placed. The scale platform model is moored by three nylon mooring lines, and the tension sensors and springs are connected between mooring lines and fairleads. A square plate is installed on the top of platform, where infrared light emit diodes (LEDs) are attached to detect the dynamic motion of platform. The light signals of LEDs are detected by a trinocular vision system, and the six rigid body motions of the floating platform are monitored. In addition, a small-size attitude and heading reference system (AHRS) manufactured by Micro-Electro-Mechanical-Systems (MEMS) Technology is attached on the top of platform to measure the acceleration, angular velocity, and attitude of the floating platform. The sensor sends the motion signals to the computer through USB (universal serial bus) port in RS-232 protocol.

The trinocular vision system consists of a trinocular camera, three infrared LEDs (light emit diodes), camera controller, and computer. The vision system, controller, and computer are placed



Fig. 4 Experimental setup for measuring the dynamic response of the moored scale model: (a) scale model (b) one-directional wave tank

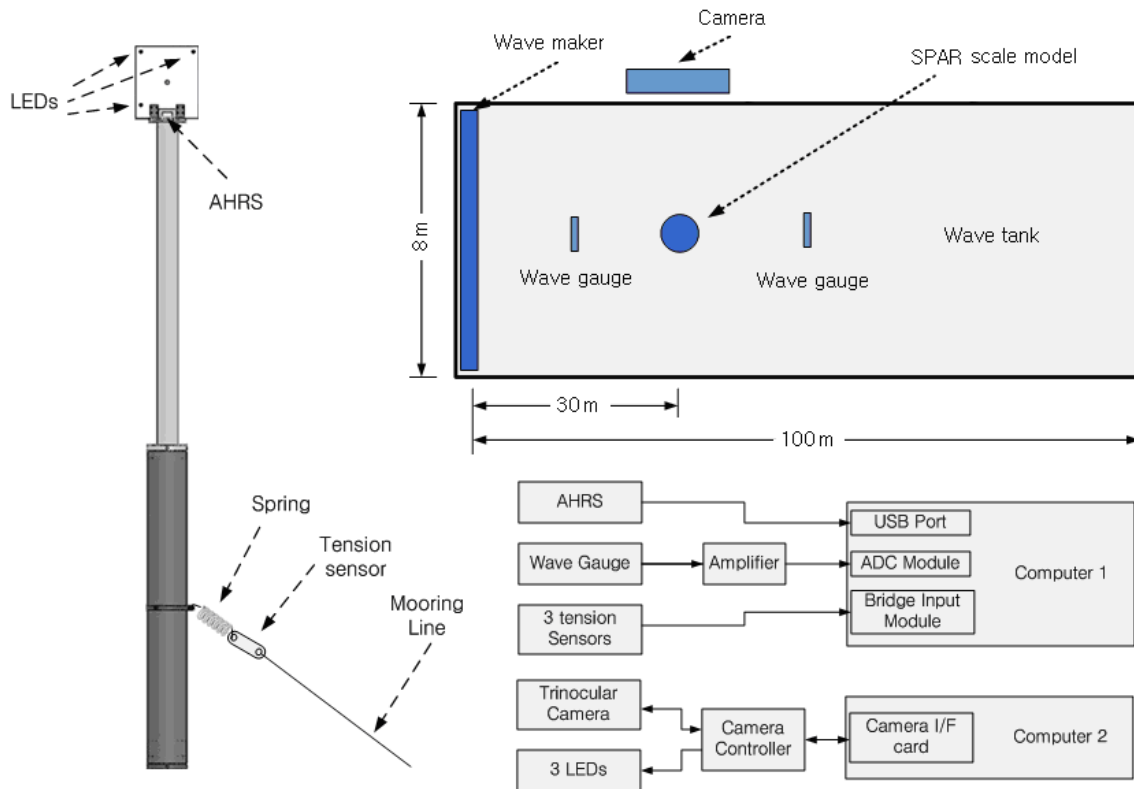


Fig. 5 Configuration of data acquisition system

on the side of the wave tank. The vision system monitors three dimensional position and attitude of the square plate. The camera controller sends the signals to the computer through the camera interface card, and the computer calculates the position and attitude of the platform in real time. Tension sensors measure the mooring line tensions, and the sensor signals are generated in the wheatstone bridge type such that the computer acquires the tension signals through a bridge input

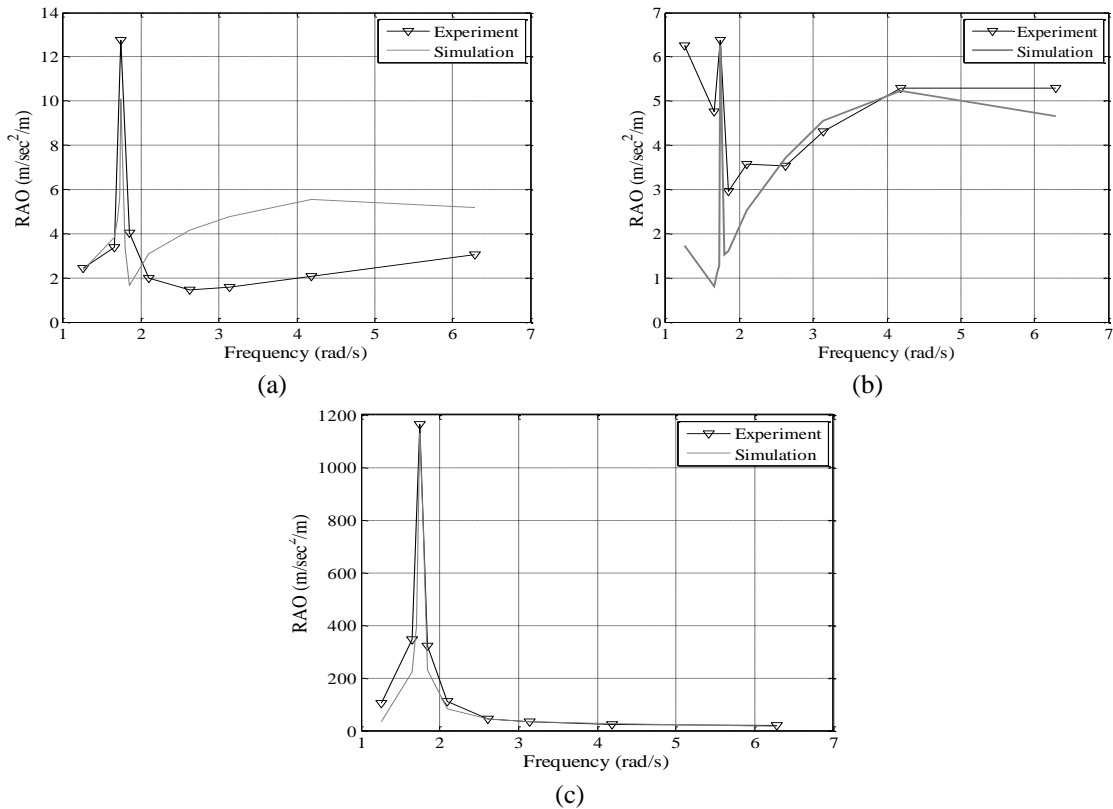


Fig. 6 RAOs of the scale model of spar floating platform: (a) surge, (b) heave, (c) pitch

module. Wave gauge is of capacitive type and immersed in the wave tank to measure the height of water wave. The signal is amplified and sent to the computer through an analog to digital converter.

Both the geometry dimensions of scale model and the test conditions are the same as the numerical simulation. Three mooring cables having the same length and pre-tension as for the numerical simulation are aligned such that one mooring line directs the incoming regular harmonic wave of the amplitude of 1.0 m and the frequency of 0.5 Hz.

#### 4. Comparison of dynamic responses

Numerical simulation and experiment are carried out and the dynamic responses in time domain are converted into frequency domain, and the response amplitude operators (RAOs) are evaluated by dividing the amplitudes in frequency domain by the wave amplitude. The loading and boundary conditions were set the same for both the numerical simulation and the experiment, in order to keep the consistency in the comparison. The one-dimensional harmonic wave specified in Section 3.1 was applied, and three linear cables were fixed at the seabed and connected to the same fairlead position of floating platform. The theories addressed in Section 2.2 were applied to the FEM model constructed by ANSYS AQWA, except for the modeling of three mooring lines. Three

mooring lines were simplified as linear cables in stead of catenary ones, so that only the cable tension was considered and interacted with the rigid body motion of floating platform.

The verification of the proposed numerical model using the experiment is made by comparing with the RAOs of rigid body motions of platform and the RAOs of two mooring lines. In fact, the dynamic responses of spar-type floating platform are evaluated mostly by these quantities. Since the wave excitation in the current study is one-dimensional harmonic in the  $x$ -direction, the dynamic responses of floating platform are characterized by surge, heave and pitch motions and the cable tension. Here, the cable tensions of only two mooring cables are taken because the cable tension of the remaining cable is almost the same with one of two mooring cables. The reader may refer to our paper (Jeon *et al.* 2013) on the parametric dynamic behavior of spar-type floating platform to the catenary mooring cables.

Fig. 6 comparatively represents RAOs of surge, heave and pitch motions of the scale floating platform, where the resonance frequencies between the numerical simulation and experiment are observed to be in excellent agreement. Thus, it is verified that the total mass, mass moments of inertia and stiffness of platform and the pre-tension and stiffness of mooring lines as well as the added mass of water are consistently reflected into the numerical simulation. Furthermore, it is observed from Fig. 6(c) that the amplitudes in pitch motion show a good agreement over all the frequency range. But, surge and heave motions show the remarkable difference in the amplitudes at high and low frequencies, respectively. But, at the resonance frequencies, the relative differences in amplitudes are found to be 20.5% in surge, 3.1% in heave and 5.3% in pitch respectively, when compared with those of experiment. From the fact that the remarkable amplitude difference occurs in surge and heave motions at high or low frequency, it is inferred that the tubular Morison element can not appropriately reflect the inertial or the restoring effect for such frequency range.

The comparison of mooring line tensions is represented in Fig. 7, where the result of line 3 is excluded due to the symmetry between lines 2 and 3. First of all, mooring line 1 exhibits higher tension than mooring line 2, which is consistent with that fact mooring line 1 aligned in the wave direction undergoes the largest extension. As in the previous RAOs of floating platform, an excellent agreement in the resonance frequencies is observed between the numerical simulation and experiment. But, it is observed that the mooring line tensions predicted by the numerical simulation are smaller than those of experiment, except for those at the resonance frequencies. At

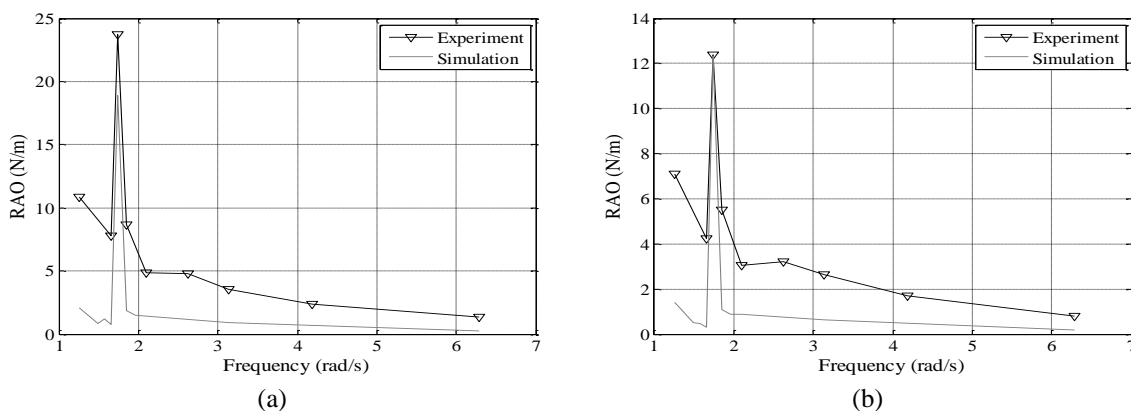


Fig. 7 RAOs of the mooring line tension: (a) line 1, (b) line 2

the resonance frequencies, the relative differences in the mooring line tension are found to be 19.88% in line 1 and 3.7% in line 2, respectively. It is inferred that the modeling of mooring lines as linear cable in which the cable tension is calculated in terms of the coordinates of its both ends predicts the mooring line tension much smaller than the experiment. Thus, the dynamic effect of mooring line is not included, and which might cause the difference between the numerical and the experimental results.

In summary, the current simulation model provides the resonant responses of the platform rigid motions and the cable tension which are consistent well with the experiment. But, it leads to the remarkable discrepancy from the experiment at the frequency ranges off the resonance frequency. It is because the current numerical model can not appropriately reflect the inertial and restoring effect of floating platform and the dynamic effect of mooring lines.

## **5. Conclusions**

A numerical method for predicting the dynamic responses of spar-type floating platform using a simplified 1/75 scale model has been addressed. The upper part composed of rotor blades, hub and nacelle were excluded from the scale model, and the time responses of surge, heave and pitch motions and the mooring line tension to one-dimensional harmonic wave were converted into frequency domain. Wave flow was modeled as linear potential flow and the wave-rigid platform interaction was simulated by a coupled FEM-cable dynamics code. The fluid viscous damping was modeled by the tubular Morison elements, and the pre-tensioned mooring lines were modeled as linear cables by specifying the unstretched initial length of cable. In order for the verification of numerical method, the experiment was performed in a wave tank by means of the specially designed sensor and data acquisition system. According to the comparison of the RAOs of surge, heave and pitch motions and the mooring line tension between the numerical simulation and experiment, the following main observations are drawn.

1. The resonance frequencies show an excellent agreement between the numerical simulation and experiment, in the RAOs of three rigid body motions and the mooring line tension over all the frequency range.

2. The amplitudes in pitch motion show a good agreement with the experiment, but surge and heave motions show the remarkable difference in the amplitudes at low and high frequencies respectively, owing to the limitation in modeling the frequency-dependent fluid damping for the numerical simulation based on the linear potential flow.

3. The mooring line tensions predicted by the numerical simulation are much smaller than those of experiment outside the resonance frequency. But, it has been observed that the relative differences between the numerical simulation and experiment are 19.88% in line 1 and 3.7% in line 2 at the resonance frequency.

## **Acknowledgements**

The financial support for this work by a 2-Year Research Grant of Pusan National University is gratefully acknowledged.

## References

- Aamo, O.M. and Fossen, T.I. (2000), "Finite element modeling of mooring lines", *Math. Comput. Simul.*, **53**(4-6), 415-422.
- ANSYS AQWA (2012), Available from: <http://www.ansys.com/products/aqwa/>.
- Cho, J.R., Lee, H.W. and Ha, S.Y. (2005), "Finite element analysis of resonant sloshing response in 2-D baffled tank", *J. Sound Vib.*, **288**, 829-845.
- Cho, J.R., Park, S.W., Kim, H.S. and Rashed, S. (2008), "Hydroelastic analysis of insulation containment of LNG carrier by global-local approach", *Int. J. Numer. Meth. Eng.*, **76**, 749-774.
- Colwell, S. and Basu, B. (2009), "Tuned liquid column dampers in offshore wind turbines for structural control", *Eng. Struct.*, **31**, 358-368.
- Cong, N.H. (1996), "Explicit parallel two-step Runge-Kutta-Nyström methods", *Comput. Math. Appl.*, **32**(3), 119-130.
- Dodaran, A.A. and Park, S.K. (2012), "Development of design static property analysis of mooring system caisson for offshore floating wind turbine", *Int. J. Ocean Syst. Eng.*, **2**(2), 97-105.
- Faltinsen, O.M. (1990), *Sea Load on Ships and Offshore Structures*, University of Cambridge.
- Goodman, T.R. and Breslin, J.P. (1976), "Statics and dynamics of anchoring cables in waves", *J. Hydron.*, **10**(4), 113-120.
- Goopee, A.J., Koo, B.J., Lambrakos, K.F. and Kimball, R.W. (2012), "Model tests for three floating wind turbine concepts", *Proceedings of Offshore Technology Conference*, Houston, USA.
- Hansen, A.D. and Hansen, L.H. (2007), "Wind turbine concept market penetration over 10 years (1995-2004)", *Wind Energy*, **10**, 81-97.
- Jensen, J., Olsen, A. and Mansour, A. (2011), "Extreme wave and wind response predictions", *Ocean Eng.*, **38**, 2244-2253.
- Jeon, S.H., Seo, M.W., Cho, Y.U., Park, W.G. and Jeong, W.B. (2013), "Study on the sloshing characteristics of annular cylindrical tuned liquid damper for spar-type floating offshore wind turbine", *Struct. Eng. Mech.*, **47**(3), 331-343.
- Jeon, S.H., Cho, Y.U., Seo, M.W., Cho, J.R. and Jeong, W.B. (2013), "Dynamic response of floating substructure of spar-type offshore wind turbine with catenary mooring cables", *Ocean Eng.*, **72**, 356-364.
- Jonkman, J. (2009), "Dynamics of offshore floating wind turbines-model development and verification", *Wind Energy*, **12**, 459-492.
- Jonkman, J. and Musial, W. (2010), "Offshore code comparison collaboration (OC3) for IEA task 23 offshore wind technology and development", *Technical Report NREL/TP-5000-48191*, Colorado.
- Karimirad, M. (2010), "Dynamic response of floating wind turbines", *Tran. B: Mech. Eng.*, **17**(2), 146-156.
- Karimirad, M., Meissonnier, Q., Gao, Z. and Moan, T. (2011), "Hydroelastic code-to-code comparison for a tension leg spar-type floating wind turbine", *Marine Struct.*, **24**, 412-435.
- Kim, J.H. and Kim, Y.H. (2001), "A predictor-corrector method for structural nonlinear analysis", *Comput. Meth. Appl. Mech. Eng.*, **191**(8-10), 959-974.
- Koo, B.J., Kim, M.H. and Randall, R.E. (2004), "Mathieu instability of a spar platform with mooring and risers", *Ocean Eng.*, **31**, 2175-2208.
- Lee, H.H., Wong, S.H. and Lee, R.S. (2006), "Response mitigation on the offshore floating platform system with tuned liquid column damper", *Ocean Eng.*, **33**, 1118-1142.
- Lee, K.H. (2005), *Response of Floating Wind Turbines to Wind and Wave Excitation*, Masters Thesis, MIT.
- Lee, S.H. (2008), "Dynamic response analysis of spar buoy floating wind turbine systems", Ph.D. Thesis, MIT.
- Lefebvre, S. and Collu, M. (2012), "Preliminary design of a floating support structure for a 5MW offshore wind turbine", *Ocean Eng.*, **40**, 15-26.
- Morison, J.R., O'Brien, M.P., Johnson, J.W. and Schaaf, S.A. (1950), "The force exerted by surface waves on piles", *Petrol. Tran.*, **189**, 149-157.
- Mostafa, M., Murai, M., Nishimura, R., Fujita, O. and Nihei, Y. (2012), "Experimental validation for motion

- of spar-type floating wind turbine at inclination with effect of gyro moment of the rotating blade of windmill”, *International Offshore and Polar Engineering Conference*, Rhodes, Greece.
- Nielsen, F.G., Hanson, T.D. and Skaare, B. (2006), “Integrated dynamic analysis of floating offshore wind turbines”, *Proceedings of 25th International Conference on Offshore Mechanics and Arctic Engineering (OMAE2006)*, **1**, 671-679.
- Shin, H. and Dam, P. (2012), “Model test of a floating offshore wind turbine moored by a spring-tensioned leg”, *International Offshore and Polar Engineering Conference*, Rhodes, Greece.
- Sigrist, J.F. and Abouri, D. (2006), “Numerical simulation of a non-linear coupled fluid-structure problem with implicit and explicit coupling procedure”, *Proceedings of ASME Pressure Vessel and Piping Division Conference*, Vancouver, Canada.
- Tong, K.C. (1998), “Technical and economic aspects of a floating offshore wind farm”, *J. Wind Eng. Indus. Aerod.*, **74-76**, 399-410.
- Tracy, C. (2007), *Parametric Design of Floating Wind Turbines*, Masters Thesis, MIT.
- Utsunomiya, T., Matsukuma, H. and Minoura, S. (2010), “On sea experiment of a hybrid SPAR for floating offshore wind turbine using 1/10 scale model”, *Proceedings of ASME 2010 29th International Conference on Ocean, Offshore and Arctic Engineering*, Shanghai, China.
- Vaz, M.A. and Patel, M.H. (2000), “Three-dimensional behavior of elastic marine cables in sheared currents”, *Appl. Ocean Res.*, **22**, 45-53.
- Wang, L. and Sweetman, B. (2012), “Simulation of large-amplitude motion of floating wind turbines using conservation of momentum”, *Ocean Eng.*, **42**, 155-164.
- Wilson, B.W. (1960), “Characteristics of anchor cables in uniform ocean currents”, Texas A&M Report No. 204-1.
- Wu.S. (1995), “Adaptive dynamic relaxation technique for static analysis of catenary mooring”, *Marine Struct.*, **8**, 585-599.
- Zambrano, T., MacCready, T., Kiceniuk, T., Goddier, D.G. and Cermelli, C.A. (2006), “Dynamic modeling of deepwater offshore wind turbine structures in gulf of Mexico storm conditions”, *Proceedings of 25th International Conference on Offshore Mechanics and Arctic Engineering*, Hamburg, Germany.